

Emergence of spin-phonon coupling in Gd-doped Y_2CoMnO_6 double perovskite oxide: a combined experimental and ab-initio study

Anasua Khan¹, Debdatta Banerjee², Divya Rawat³, T.K Nath¹, Ajay Soni³,
Swastika Chatterjee², and A.Taraphder¹

¹*Department of Physics, Indian Institute of Technology, Kharagpur-721302, West Bengal, India*

²*National Centre for High-Pressure Studies and Department of Earth Sciences, Indian Institute of
Science Education and Research Kolkata, Nadia- 741246, West Bengal, India*

³*School of Physical Sciences, Indian Institute of Technology Mandi, Mandi-175005, Himachal Pradesh,
India*

Abstract

One of the fundamental interactions that is found in many functional materials is the spin-phonon coupling (SPC), which is at the heart of many novel functionalities. The simultaneous presence of multi-magnetic phases makes SPC even more intriguing. We have used Raman spectroscopy as well as first-principles methods to investigate the possibility of the appearance of spin phonon coupling (SPC) in Gd-doped Y_2CoMnO_6 (YGCMO) double perovskite oxide and the influence of anti-site disorder on the same. YGCMO exhibits anti-site disorder leading to both ferromagnetic (between Co and Mn) and anti-ferromagnetic interactions (Co-Co, Mn-Mn, Gd-Co/Mn), making the SPC more intriguing. An analysis of the temperature-dependent phonon frequency for the stretching modes of YGCMO indicates that SPC is possibly emerging from simultaneous presence of ferromagnetic and antiferromagnetic interactions. The spin-phonon coupling strength comes out to be 0.29 cm^{-1} . Our experimental findings are corroborated by first-principles density functional theory (DFT) based

calculations which indicate that SPC in YGCMO gets enhanced in the presence of anti-site disorder. This implies a strong influence of B-site (Co/Mn) ordering on SPC in the bulk double perovskite systems. Thus, the phonon dynamics of YGCMO are strongly correlated with magnetic ordering. This material has potential applications in spintronics devices.

1 Introduction

Multifunctional materials with correlated electronic structures have of late witnessed a surge in interest due to their inherent fundamental physics [1] (like frustrated magnetism and various spin states) and potential devices application (such as memories [2] and spintronics [3]). The strong correlation between the spin, charge, orbital, and lattice degrees of freedom is responsible for such emergent properties [4, 5]. In this regard, the compounds with the generic formula R_2BMnO_6 (R= rare earth B = transition metal) have been found to hold great promise.

In general, the ordered double perovskite (DP) R_2BMnO_6 materials are found to be ferromagnetic (FM) in nature by virtue of the B^{2+} -O- Mn^{4+} superexchange interaction [6, 7]. Previous experimental and theoretical research on this class of materials reports the emergence of several novel functionalities, namely, magnetocapacitance, magnetoresistance, relaxor ferroelectricity, and multiferroicity [9, 10, 11, 12]. Besides, the nature of order/disorder at the B and Mn sites in these DP materials has been found to greatly influence the electronic, magnetic, vibrational, and dielectric properties [13, 14, 15, 5, 16]. Anti-site disorder (ASD) may also result in the suppression of ferromagnetism in some materials. This is because ASD induces B^{2+} -O- B^{2+} and Mn^{4+} -O- Mn^{4+} super-exchange interactions, which results in short range anti-ferromagnetic (AFM) interactions [28].

Recently the DPs containing smaller rare earth cations have been of great research interest as many theoretical, as well as experimental studies report the emergence of novel multiferroic properties [18] in these materials. Of particular interest is the Y-based double perovskite such as Y_2CoMnO_6 (YCMO) and Y_2NiMnO_6 , which have been found to exhibit polar nature in their magnetic ground state [19]. Moreover, first-principles calculations have shown that YCMO double perovskite oxides develop E^* type magnetic ordering which is the source of ferroelectricity in these

materials [20, 21]. It also exhibits some interesting properties like disorder-induced exchange bias and other multiferroic properties [28].

In a strongly correlated system, the richness of the novel functionalities depends on the coupling of magnetic spins, the crystal lattice, and lattice vibrations. The interaction is complex but rich in the case of DP materials as it has two different magnetic species. So, a qualitative model based on spin-phonon coupling was proposed earlier for YCMO [22] in order to explain magnetically induced ferroelectricity in this material. SPC provides a fundamental background to understand various phenomena, such as magneto-thermal transport, magnetoelectric coupling, thermal Hall Effect, relaxation time in spintronics, etc. [23]. Spin-phonon coupling also facilitates the design of different spintronic devices with low-power and high-speed operations [?]. For instance, external magnetic fields are used to regulate magnetic refrigeration, isothermal entropy, and adiabatic temperature [?]. Furthermore, SPC also provides a chance to modulate the functionality of transition metal oxides (TMO) [25]. It is now well-understood that the coupling of phonons with other degrees of freedom may play a vital role in dictating several properties of these systems. In the past several studies have delved into the electronic, magnetic, optical, and transport properties of DP systems, phonon-related phenomena and their interactions with other degrees of freedom have not yet been thoroughly investigated. [5, 13]. Hence, an investigation of the nature of the “coupling” is crucial for understanding these systems better.

Interestingly, the spin- phonon coupling of DP system can be changed with lattice parameters such as cationic size, bond length, and bond angle [24]. Kumar *et al.* investigated that the SPC value gets weakened with the decrease in ionic radius of A-site cation in DP thin film [24]. This is related to the induced chemical pressure (large octahedral distortion) in the system, which modifies the FM superexchange interaction due to decrease in bond length of TM ions. On the other hand, Co-based DP compound LCMO exhibits SPC in thin films, whereas phonon modes remain unaffected due to change in magnetic ordering in bulk sample [26].

In this study, we have replaced 50% Y^{3+} ions with magnetic rare earth Gd^{3+} ions [28] to account for the effect of both local distortion and magnetism on SPC in YGCMO compound. For this purpose, temperature-dependent Raman spectroscopy along with first-principles DFT calculations are employed to investigate SPC in this DP compound [27]. It can also unveil the origin of SPC,

whether it is direct or due to magnetostriction.

2 Experimental and Computational Details

The polycrystalline, single-phase double perovskite sample of $Y_{1-x}Gd_xCoMnO_6$ ($x=0.5$) (YGCMO) was synthesized by the well-known chemical sol-gel method. A detailed description of sample preparation can be found in section S1 of the supplementary information (SI).

Raman scattering measurements were performed using Horriba Jobin Vyon LabRAM HR Evolution Raman spectrometer equipped with Czerny-turner grating (1800 gr/mm), 633 nm laser excitation of 1.25 mW power, 60s acquisition time, and Peltier cooled CCD detector. Low temperature-dependent Raman measurements were performed using a Montana cryostat in the temperature range of 4-300 K with the temperature step 20 K. An ultra-low frequency filter was used to access low-frequency Raman modes. All the spectra were fitted by the Lorentzian function to evaluate the phonon frequency of the Raman modes.

The detailed structural and magnetic study on YGCMO has been done in our previous paper [28] which reveals that the compound crystallizes in monoclinic symmetry as a prime phase (99.42%) [28]. It is partially disordered with Co^{2+} , Co^{3+} , Mn^{3+} and Mn^{4+} ions. An appreciable amount (38%) of antisite disorder is found in this sample. It exhibits three different magnetic transitions: i) FM transition triggers at $T_C=95.5$ K due to Co^{2+} -O- Mn^{4+} superexchange interaction. ii) Antiferromagnetic (AFM) transition occurs at $T_N=47$ K due to $3d-4f$ exchange interaction of Co/Mn and Gd sublattices and ASD disorder present in the sample. iii) At $T\leq 20$ K, Gd^{3+} -O- Gd^{3+} interactions become active and give rise to AFM interactions. More details are found in SI (refer to Fig.S1).

All theoretical calculations have been performed using first principles density functional theory (DFT) [29, 30] using projector augmented wave method (PAW) [31, 32] as implemented in the VASP code [33, 34]. The Perdew-Burke-Ernzerhof (PBE) [35] formalism of the generalized gradient approximation (GGA) has been used as the exchange correlation functional in our calculations. An energy cut-off of 550 eV and kpoint mesh of $6\times 6\times 6$ was applied using the Monkhorst-Pack method [36]. The energy convergence with respect to all computational parameters was ascertained. A complete optimization of the crystal structure was performed till the forces were less than 0.001

eV/Å. In order to take into account, the missing correlation beyond GGA, a supplemented GGA+U calculation was performed with the U-J (U: on-site Coulomb repulsion; J: Hunds coupling strength) [37] value as 3 eV for Co-d, 3 eV for Mn-d [13] and 6 eV for Gd-f-orbitals [28]. Phonon frequencies and eigen vectors were determined from the dynamical matrices which were in turn determined from the force constants obtained using density functional perturbation theory (DFPT) [38] as implemented in VASP and post-processed using PHONOPY [39].

3 Results and discussion

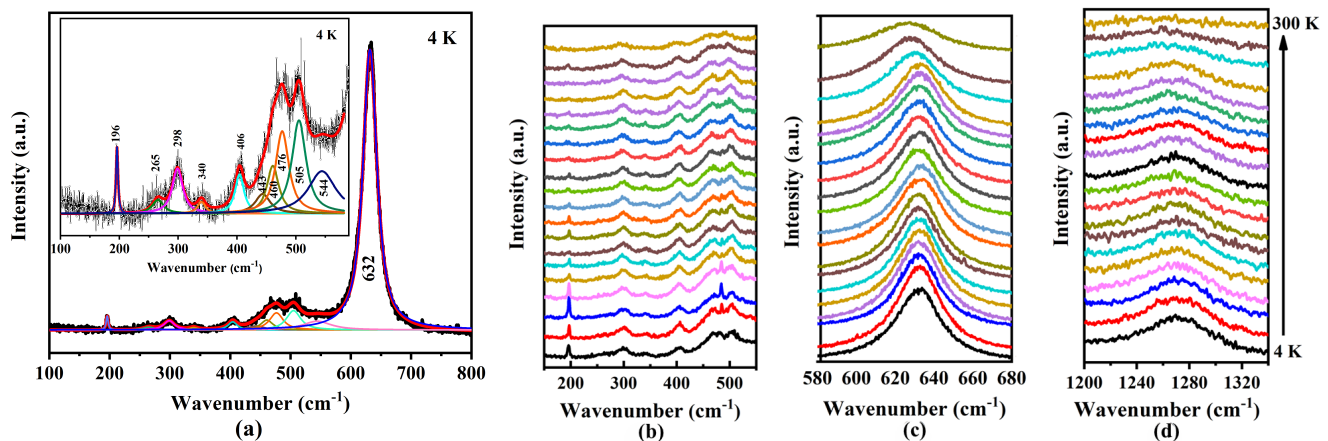


Figure 1: Raman spectra of Gd-doped YCMO at (a) 4 K. The inset shows low wavenumber region. The red solid line shows the net fitted spectrum and blue, green, orange, cyan, and brown lines correspond to individual peaks. Temperature-dependent Raman spectra in the (b) low wavenumber region, (c) main vibrational mode, and (d) high wavenumber region.

The irreducible representation of the possible Raman modes of Gd-substituted YCMO at $T=4$ K is shown in Fig. 1(a). The absence of most intense Raman peak of Y_2O_3 near 377 cm^{-1} [40, 41] indicates the absence of a secondary phase (RE_2O_3) [42] in the system. Fig. 1(a) depicts eleven first-order Raman modes resolved at $T=4$ K, and their frequencies are determined by deconvoluting the spectrum with the Lorentzian line profile. However, no structural phase transition is observed throughout the temperature variation, confirming that the YGCMO remains in a monoclinic structure with space group $P2_1/n$, shown in Fig. 1 (b), (c), and (d). In this symmetry, $4e$ sites are generally occupied by the rare earth ions and oxygen atoms, whereas Co and Mn ions prefer $2c$ and $2b$ sites, respectively. The schematic of the structure is shown in Fig. 5.

The low symmetry structures of double perovskites result from a distorted cubic $Fm\bar{3}m$ aristo-

type lattice [43]. From the group theory calculation, 24 Raman active modes are expected to be observed for this space group. Its distribution according to the irreducible representation of $2/m$ factor point group is given as follows: $6T(3A_g + 3B_g) + 6L(3A_g + 3B_g) + 2\nu_1(A_g + B_g) + 4\nu_2(2A_g + 2B_g) + 6\nu_5(3A_g + 3B_g)$, which can be written as $12A_g + 12B_g$ [27]. Lattice modes (T = translational and L = librational) are observed below 380 cm^{-1} whereas internal modes corresponding to oxygen octahedron (ν_1, ν_2 , and ν_5) are detected above 380 cm^{-1} [27]. Generally, vibrational modes correspond to oxygen atoms connected with higher valence ions [44]. In this experiment, out of 24 Raman active modes, 11 Raman modes can be resolved at $T = 4 \text{ K}$ which is notably larger than the resolved mode for other La-based double perovskites [15, 27]. Smaller ionic radii of Y^{3+} and Gd^{3+} cation ($r = 1.20 \text{ \AA}$ and $r = 1.22 \text{ \AA}$) in YGCMO lead to more distortion in the structure, which results in major octahedra tilts. As a consequence, a significant number of modes have been observed. In comparison with LCMO, the Raman bands split more for YGCMO due to strong monoclinic distortion [45].

In the past, Iliev *et al.* [27] have identified the Raman modes for Mn-based DP system from the semiempirical calculation, and it is in good agreement with their experimental results. Therefore, based on some of the previous works [27, 46], Raman modes at 632 cm^{-1} , 505 cm^{-1} , 340 cm^{-1} , 298 cm^{-1} , 265 cm^{-1} , and 196 cm^{-1} observed in our experiment can be assigned to A_g symmetry and also known as stretching mode (S). Here Co/Mn-O bond involves both in-plane and out-of-plane vibrations and those detected at 544 cm^{-1} , 476 cm^{-1} , and 406 cm^{-1} have B_g symmetry and are also known as anti-stretching mode (AS). Here O^{2-} ions vibrate perpendicularly to the Co/Mn-O bond. The mode noticed at higher wave number 1270 cm^{-1} corresponds to the second-order overtone of breathing mode [47].

In order to study spin-phonon coupling in our sample, the effect of temperature on the phonon modes has been analyzed. The recorded temperature dependence of the Raman spectrum between 4 K and 300 K is shown in Fig. 1 (b), (c), and (d). These figures illustrate the impact of magnetic ordering on the lattice vibration. Generally, in manganite perovskite, the stretching mode shows spin-phonon coupling [48]. In our study, the temperature dependence of two of the most representative Raman modes are presented in Fig. 2 (a-b). Temperature dependence of phonon frequency due to anharmonic contribution (due to lattice contraction) proposed by Balkanski [49] can be written

as follows,

$$\omega(T) = \omega(0) - C \left(1 + \frac{2}{e^{\frac{\hbar\omega_0}{kT}} - 1} \right) \quad (1)$$

where C (anharmonic constant) and ω_0 (position of the Raman mode at the temperature $T=0$

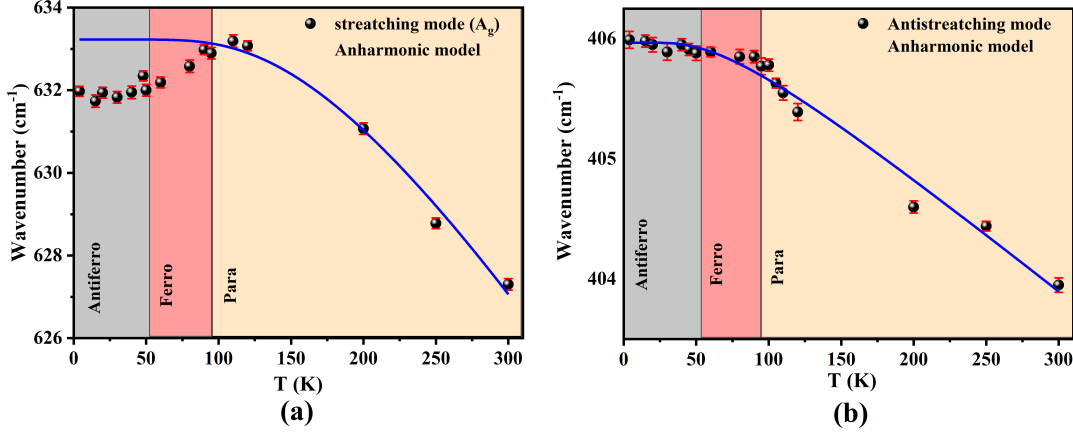


Figure 2: Temperature-dependence of phonon positions of (a) A_g stretching mode, (b) B_g anti-stretching mode for YGCMO (black sphere). The blue line represents the approximation from the above anharmonic model. The error bars are the standard deviation of the peak positions as obtained from the fitting procedure.

K) are the adjustable parameters. In the absence of any phase transition, temperature-dependent Raman mode should follow the above anharmonic relation. It is seen that the most intense Raman mode, also known as stretching mode (observed at 632 cm⁻¹), fits nicely with the anharmonic model above T_C , shown in Fig. 2(a). This mode shows a deviation from the above model for $T \leq T_C$ with two distinct discontinuities at T_C and T_N , respectively. The deviation is more pronounced with lowering the temperature. This anomalous behavior could arise due to the renormalization of phonons induced by the ferromagnetic ordering of Co-Mn ions and results in the coupling between spin and lattice (phonon) degrees of freedom [50]. A similar feature is observed in several double perovskite manganite systems [51, 52]. On the other hand, the AS Raman mode observed at 406 cm⁻¹, fits well with the above anharmonic model throughout the investigated temperature range except near T_C . At lower temperatures, the phonon frequencies become nearly constant for this mode. This temperature-independent behavior of phonon frequencies at lower temperatures could happen due to a change in magnetic spin structure or weak ferromagnetic ordering [53]. Our previous study shows that below T_{Gd} (Gd ordering temperature), Gd spins are at ab plane, which was in c direction [28].

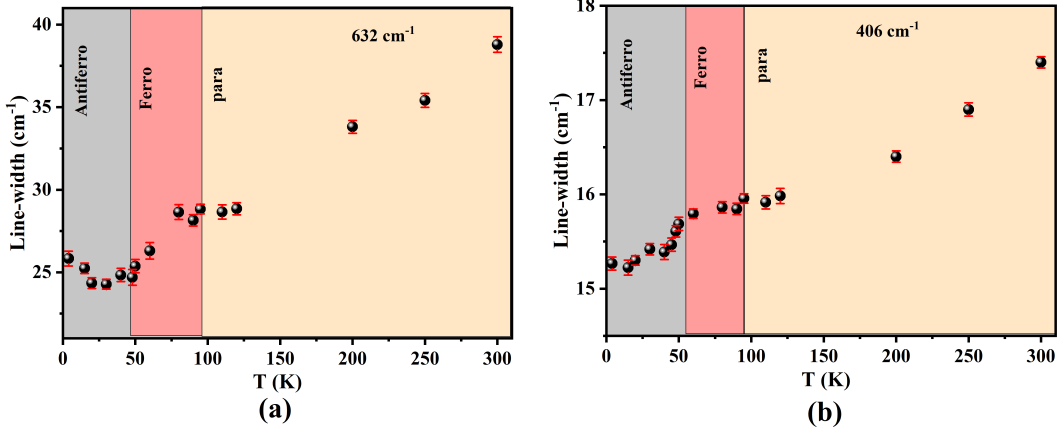


Figure 3: Temperature-dependence of Raman line width (FWHM) of (a) A_g mode, and (b) B_g mode. The error bars are the standard deviation of the peak positions as obtained from the fitting procedure.

The temperature dependence of linewidth of stretching and anti-stretching modes are plotted in Fig. 3 (a-b) to investigate the role of magnetostriction in this coupling. Raman linewidth is associated with phonon life-time that is not affected by lattice volume changes i.e. magnetostriction effect. Generally, a significant anharmonic effect has been observed at higher temperatures due to rigorous atomic vibration of the atoms about their mean position. However, this anharmonic effect gets reduced with a decrease in temperature due to reduced phonon-phonon interactions. As a result, phonon-lifetime increases or FWHM decreases. We observed that both the curves show anomaly upon entering into the magnetic region with the discontinuities at 95.5 K (T_C) and 47 K (T_N), respectively, which suggests relative dependence of phonon lifetime with magnetic ordering. Therefore, strong interaction between phonon and magnetic degree of freedom leads to an increase in linewidth at lower temperatures i.e., a decrease in phonon lifetime. Usually, the linewidth is affected by spin-phonon coupling and electron-phonon coupling [59]. The total electronic density of states for YGCMO shows that it is insulating in nature (refer to Fig.S2 in SI). Therefore, the anomaly in linewidth with temperature is ascribed to spin-phonon coupling [59].

The careful observation of the above temperature-dependent frequency and linewidth plot reveals a new phonon renormalization arising at T_N due to AFM ordering of Gd-Co/Mn spins, implying the presence of spin-phonon coupling. This result suggests that the FM phase i.e. ordered regions and similar disordered clusters exist together in this sample, where the predominant AFM interactions are produced from $\text{Co}^{3+}\text{-O- Co}^{3+}$, $\text{Mn}^{3+}\text{-O-Mn}^{3+}$, $\text{Co}^{2+}\text{-O- Co}^{2+}$, $\text{Mn}^{4+}\text{-O-Mn}^{4+}$, and $3d\text{-}4f$ exchange pathways. Besides magnetic measurements, Raman spectroscopy is a powerful tool to

detect magnetic inhomogeneity present in the sample.

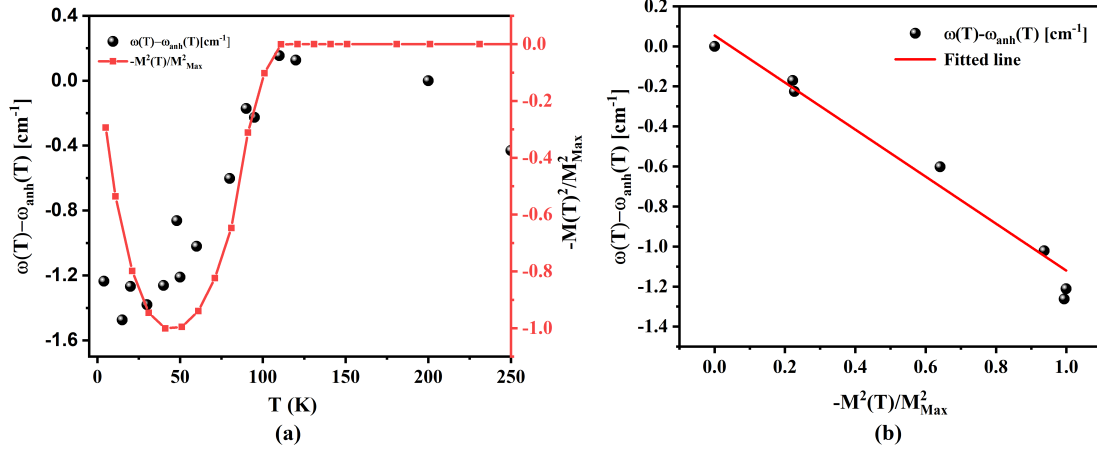


Figure 4: (a) A comparison of the deviation ($\Delta\omega(T)$) of A_g stretching mode from the anharmonic model and the normalized magnetization $\frac{M^2(T)}{M_{max}^2}$. (b) the corresponding linear dependence of $\Delta\omega(T)$ on the squared relative magnetisation $\frac{M^2(T)}{M_{max}^2}$.

To get detailed insight into the anomalous behavior of Raman modes, the renormalization of phonon frequency with normalized magnetic moment has been plotted in Fig. 4(a). Usually, the deviation of phonon mode from the anharmonic model can be explained by the spin-spin correlation function in magnetic oxides [26].

$$\Delta\omega_{SPC}(T) = \omega(T) - \omega_{anh}(T) \approx -\lambda \langle \mathbf{S}_i \cdot \mathbf{S}_j \rangle \quad (2)$$

where $\omega(T)$ is the normalized phonon frequency due to SPC, ω_{anh} is the phonon frequency in the absence of SPC, S_i and S_j are nearest neighbor spins at i^{th} and j^{th} sites, respectively. λ denotes the strength of spin-phonon coupling. $\Delta\omega$ is obtained by taking the difference between calculated and observed phonon frequencies. According to mean-field theory, the spin-spin correlation function can be connected to magnetization by the equation $\Delta\omega_{SPC} \approx (M(T)/M_{max})^2$, where $M(T)$ and M_{max} are the magnetization at T and saturation magnetization approximated to $T=0$ K, respectively. Therefore, by considering the four nearest neighbors for each B site cation, $\Delta\omega_{SPC}$ can be written as follows [56]:

$$\Delta\omega_{SPC} \approx -\lambda \langle \mathbf{S}_i \cdot \mathbf{S}_j \rangle \approx -4\lambda \frac{M^2(T)}{M_{max}^2} \quad (3)$$

The spin-phonon coupling constant value λ is estimated by using the above approach. Its value can

be positive or negative depending upon phonon hardening or softening. In Fig. 4(a), it is seen that there is a good overlap of both $\Delta\omega_{SPC}$ and normalized magnetization $\frac{M^2(T)}{M_{max}^2}$ up to 95 K, after that a deviation in the magnitude of $\Delta\omega_{SPC}$ occurs. It signifies that the origin of anomalous softening is ascribed to spin-phonon coupling. The occurrence of this unconventional behavior below 95 K might be caused by competition between FM and AFM interactions due to ASD present in the sample. ASD helps to originate different types of AFM ($\text{Co}^{2+}\text{-O-Co}^{2+}$, $\text{Mn}^{4+}\text{-O-Mn}^{4+}$, etc.) along with FM ($\text{Co}^{2+}\text{-O-Mn}^{4+}$) interactions, leading to magnetic frustration in the systems. In our sample, another source of AFM is the interaction between Co/Mn and Gd sublattices. Therefore, different values of magnetic coupling J_{ij} can contribute in different ways to the phonon renormalization induced by magnetic ordering. It makes the spin-phonon coupling more complex and causes deviation from mean field approximation. A similar kind of deviation is observed in $\text{La}_2\text{CoMnO}_6$ [55], $\text{Gd}_2\text{CoMnO}_6$ [56], and $\text{Lu}_2\text{CoMnO}_6$ [57], where FM and AFM interactions coexist together.

Spin-phonon coupling strength (λ) is determined by taking a quarter of the slope of the linear relationship of $\Delta\omega_{SPC}$ vs. $\frac{M^2}{M_{max}^2}$ [24] shown in Fig. 4 (b). The value is found to be 0.29 cm^{-1} . It has been observed that SPC value is always lower for bulk sample than thin film [26] because epitaxy stress plays pivotal role towards SPC. Silva *et al.* reveal that ordered bulk LCMO does not show SPC whereas disordered GCMO exhibits SPC to a greater extent [60]. Again, Meyer *et al.* [26] show that spin-phonon coupling coefficient value is lower for disordered LCMO in thin film than the ordered one. Thus B-site cationic ordering has not only influenced the magnetic properties of YGCMO perovskite significantly but also affects its phonon properties and spin-phonon coupling strength λ to a great extent.

SPC in the YGCMO compound is further investigated by first-principles calculations. We have considered a supercell of size $1 \times 2 \times 1$ containing 40 atoms i.e, there are 4 Y, 4 Gd, 4 Co, 4 Mn, and 24 O atoms in each supercell. The structure was fully optimized, starting from the room temperature experimental data. Fig. 5(a) shows the lowest energy ordered structure of YGCMO where Co and Mn octahedra are arranged alternately. To determine the influence of anti-site disorder on the nature of SPC, starting from the ordered $1 \times 2 \times 1$ crystal structure, we have manually introduced some anti-site disorder. This disordered structure thereafter underwent a complete optimization (see Fig. 5 (b)). The total electronic density of states for the disordered structure (which contains Co-Co, Co-Mn, and Mn-Mn interactions) shows that the sample is insulating with a band gap of 1

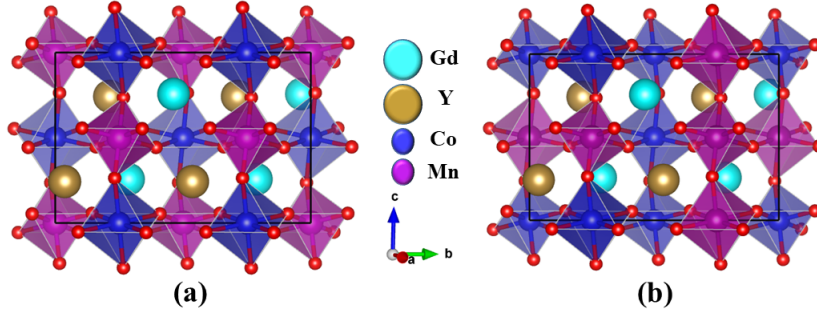


Figure 5: Lowest energy crystal structure of (a) ordered YGCMO and (b) disordered YGCMO. The blue and purple balls represent Co and Mn atoms respectively, and sit at the centre of the octahedra. Here Y and Gd atoms are represented by golden and cyan big balls, sitting in the cage formed by CoO_6 and MnO_6 octahedra.

eV (refer to Figure S2 of the SI). To determine the magnetic ground state, we have performed total

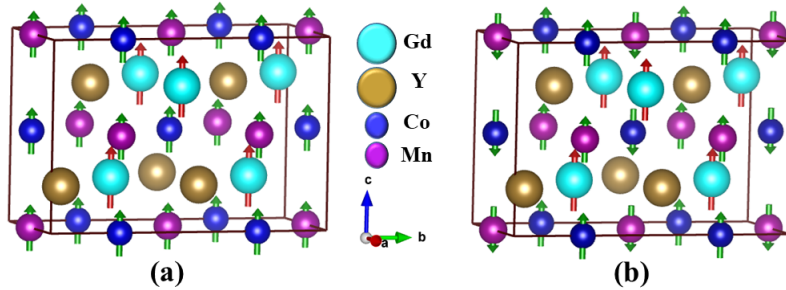


Figure 6: Energetically preferred spin configurations of ordered YGCMO (a) Ferromagnetic ordering; (b) C-type AFM ordering. Here, blue, and purple small balls and golden and cyan big balls represent Co, Mn, Y, and Gd atoms respectively. The red arrows denote the spins on Gd atoms and green arrows represent the spins on Co and Mn atoms.

energy calculations on the ferromagnetic, C-, G-, and A-type antiferromagnetic and ferrimagnetic configurations of ordered-YGCMO. These magnetic interactions were considered among the Co and Mn ions, whereas the Gd moments were made to orient along the z-direction in all the calculations. Our calculations indicate that the ferromagnetic state (see Fig. 6(a)) has the lowest energy followed by the C-type AFM magnetic configuration (see Fig. 6 Y(b)). The relative energies of the different magnetic orderings with respect to the ferromagnetic state have been tabulated in Table 1. To investigate whether there is a coupling between the spin and the lattice degrees of freedom, we have calculated the total phonon density of states for the two lowest energy magnetic configurations, namely, the ferromagnetic and the C-type antiferromagnetic state, in both its ordered and anti-site disordered state (as shown in Fig. 5). The total phonon density of states for these two configurations is shown in Fig. 7. The absence of imaginary modes affirms the dynamical stability of both the

Table 1: Total energy of different magnetic configurations of ordered YGCMO with respect to the ferromagnetic state.

Spin configurations	Relative energy values (eV/f.u.)
FM	0.0
C-type AFM	0.214
G-type AFM	0.259
A-type AFM	1.863
Ferrimagnetic	0.252

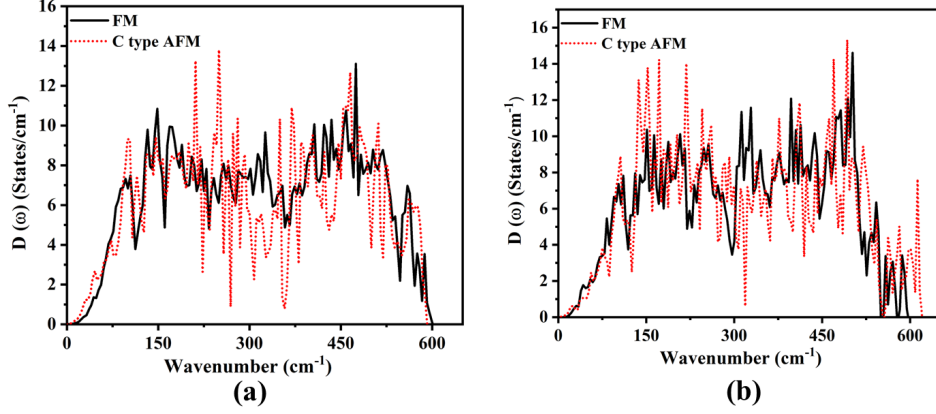


Figure 7: Comparative total phonon density of states of FM and C-type AFM for (a) ordered state, (b) disordered state.

magnetic configurations. It is evident from Fig. 7(a) that with the change in magnetic ordering, there is an alteration in the phonon density of states, indicating that spin-phonon coupling is active in this system. The partial phonon density of states for FM and C-type magnetic configuration is presented in Figure S3 of the SI. We have also checked the influence of disorder at Co and Mn on the spin-phonon coupling, as presented in Fig. 7(b). Our calculations indicate that with the introduction of disorder in the system, the shift between prominent modes further increases approximately by 3%. To investigate the cause behind the enhanced spin-phonon coupling in the case of disordered YGCMO, we performed a detailed structural analysis of the sample in the presence/absence of disorder. It was observed that in the ordered sample the Co-O-Mn bond angle was enhanced by 0.46° as the magnetic configuration was changed from FM to C-type. However, the same was found to be reduced by 1.88° for the disordered sample (refer to Table 2). Analysis of the bond lengths of the CoO_6 and MnO_6 octahedra showed that in ordered YGCMO the average Co-O bond length is found to increase by 0.0117 \AA and the average Mn-O bond length was found to decrease by 0.0044 \AA (refer to Table 3) as the magnetic configuration was changed from FM to C-type AFM.

Table 2: The average bond angles between transition metal elements obtained from DFT calculations are as follows

	Co-O-Mn ($^{\circ}$)	Co-O-Co ($^{\circ}$)	Mn-O-Mn ($^{\circ}$)
FM-ordered	144.85	-	-
C-type AFM-ordered	145.31	-	-
FM-disordered	146.66	147.28	145.16
C-type AFM disordered	144.78	145.09	144.82

Table 3: The average bond length of Co-O and Mn-O obtained from DFT are as follows

	Co-O (\AA)	Std. deviation (\AA)	Mn-O (\AA)	Std. deviation (\AA)
FM-ordered	2.0809	0.00	1.9444	0.00
C-type AFM-ordered	2.0926	0.0011	1.9400	0.0006
FM-disordered	2.0426	0.05537	1.9731	0.02856
C-type AFM disordered	2.0447	0.05997	1.9567	0.04715

On the contrary, for similar magnetic transformations, both the average Co-O and Mn-O bond lengths were found to get enhanced and reduced by 0.0021 \AA and 0.0164 \AA , respectively (refer to Table 3). However, there is in general an increase in the distortion of the CoO_6 and MnO_6 octahedra with change in magnetic ordering, which is found to increase with the introduction of anti-site disorder. It has been observed previously [61] that the relation between the frequencies of the RAMAN modes (ν) and the bond length (l) is $\nu = 1/\sqrt{l}$. Therefore, the modulation in bond length of a specific atom engaged with a particular vibration can lead to shifts in mode positions. This is also evident in our first-principles calculations which show that in the presence of anti-site disorder, the magnetism induced distortion of the lattice is more which eventually gets reflected in the phonon spectra.

4 Conclusion

In summary, temperature-dependent Raman study confirms that the sample holds its $P2_1/n$ symmetry throughout the investigating temperature range. Anomalous softening of A_g stretching mode implies the appearance of SPC due to the presence of both FM and AFM interactions. Again, the nature of phonon linewidth curves and the insulating nature of the material discards the effect of magnetostriction on the observed softening of A_g mode. On the other hand, shift in mode position from the anharmonic approach exhibits an unconventional behavior towards the square of the

magnetization. This is because of competing FM and AFM magnetic ordering, which is driven by ASD. The calculated value of the SPC strength is found to be 0.29 cm^{-1} . Our DFT based first-principles calculations indicate the presence of SPC in both ordered and disordered YCMO. Interestingly, SPC is found to be enhanced in the presence of anti-site disorder at the Co/Mn sites. Microscopic analysis indicates the intricate relationship between magnetism, state of orderliness at the crystallographic sites and the crystal structure of the YGCMO sample. Such materials are known to hold great promise in the field of spintronics.

5 Acknowledgments

AK acknowledges the University Grants Commission (UGC) and the Ministry of Education (MoE) for their financial support. AK, AT, and TKN also acknowledge the National Supercomputing Mission (NSM) for providing computing resources of PARAM Shakti at IIT Kharagpur, which is implemented by C-DAC and supported by the Ministry of Electronics and Information Technology (MeitY) and Department of Science and Technology (DST), Government of India. AS would like to thank the IIT Mandi for research facilities. DB acknowledges funding from the Prime Minister's Research Fellowship scheme (PMRF) and computing facilities of IISER Kolkata. SC acknowledges funding through the IISER Kolkata start-up grant and SERB-POWER Grant (Grant No.: SPG/2021/003842).

References

- [1] W. Eerenstein, N. D. Mathur, and J. F. Scott, *Nature (London)* **442**, 759 (2006).
- [2] J. F. Scott, *Nat. Mater.* **6**, 256 (2007).
- [3] I. Zutic, J. Fabian, and S. D. Sarma, *Rev. Mod. Phys.* **76**, 323 (2004).
- [4] J. K. Murthy, K. D. Chandrasekhar, H. C. Wu, H. D. Yang, J. Y. Lin, and A. Venimadhav, *Journal of Physics: Condensed Matter* **28**, 086003 (2016).
- [5] R. I. Dass and J. B. Goodenough, *Phys. Rev. B* **67**, 014401 (2003).

- [6] R.J. Booth, R. Fillman, H. Whitaker, A. Nag, R.M. Tiwari, K.V. Ramanujachary, J. Gopalakrishnan and S.E. Lofland. *Mater. Res. Bull.* **44**, 1559–64 (2009).
- [7] J.B. Goodenough. *Phys. Rev.* **100**, 564 (1955).
- [8] N.S. Rogado, J. Li, A.W. Sleight, M.A. Subramanian, *Adv. Mater.* **17**, 2225–2227 (2005).
- [9] K.D. Chandrasekhar, A.K. Das, A. Venimadhav, *J. Phys. Condens. Matter.* **24**, 376003 (2012).
- [10] P.R. Mandal, A. Khan, T.K. Nath, *J. Appl. Phys.* **128**, 024104 (2020).
- [11] I. Álvarez-Serrano, M.L. López, F. Rubio, M. García-Hernández, G.J. Cuello, C. Pico, M. Luisa Veiga, *J. Mater. Chem.* **22**, 11826 (2012).
- [12] M.G. Masud, A. Ghosh, J. Sannigrahi, B.K. Chaudhuri, *J. Phys. Condens. Matter.* **24**, 295902 (2012).
- [13] A. Khan, S. Chatterjee, T.K. Nath and A. Taraphder, *Phys. Rev. B* **104** 035152 (2021).
- [14] R.X. Silva, A.S. Menezes, R.M. Almeida, R.L. Moreira, R. Paniago, X. Marti, H. Reichlova, M. Mary, M. Vinicius, S. Rezende, C.W.A. Paschoal, *J. Alloys Compd.* **661**, 541–552 (2016).
- [15] K.D. Truong, J. Laverdière, M.P. Singh, S. Jandl, P. Fournier, *Phys. Rev. B.* **76** (2007) 132413.
- [16] A.J. Barón-González, C. Frontera, J.L. García-Muñoz, B. Rivas-Murias, J. Blasco, *J. Phys. Condens. Matter.* **23**, 496003 (2011).
- [17] A. Dias, L.A. Khalam, M.T. Sebastian, C. William, C.W.A. Paschoal, R.L. Moreira, *Chem. Mater.* **18**, 214–220 (2006).
- [18] I. O. Troyanchuk, D. D. Khalyavin, J. W. Lynn, R. W. Erwin, Q. Huang, H. Szymczak, R. Szymczak and M. J. Baran. *Appl. Phys.* **88**, 360 (2000).
- [19] M. H. Tang, Y. G. Xiao, B. Jiang, J. W. Hou, J. C. Li, and J. He, *Appl. Phys. A* **105**, 679 (2011).
- [20] S. Kumar, G. Giovannetti, J van den Brink and S. Picozzi , *Phys. Rev. B* **82** 134429 (2010).

- [21] S. Picozzi, Kunihiro Yamauchi, Ivan A Sergienko, Cengiz Sen, Biplab Sanyal, Elbio Dagotto. *J. Phys.: Condens. Matter* **20**, 434208 (2008).
- [22] G. Sharma, J. Saha, S.D. Kaushik, V. Siruguri, S. Patnaik, *Appl. Phys. Lett.* **103**, 012903 (2013).
- [23] X. Moya & N.D. Mathur. *Nat. Mater.* **16**, 784–785 (2017).
- [24] D. Kumar, S. Kumar and V. G. Sathe, *Solid State Commun.* **194**, 59 (2014).
- [25] R. Ramesh & N.A. Spaldin. *Nat. Mater.* **6**, 21–29 (2007).
- [26] Ch. Meyer, V. Roddatis, P. Ksoll, B. Damaschke, and V. Moshnyaga *Phys. Rev. B* **98**, 134433 (2018).
- [27] M. Iliev, M. Abrashev, A. Litvinchuk, V. Hadjiev, H. Guo, and A. Gupta, *Phys. Rev. B* **75**, 104118 (2007).
- [28] A. Khan, S. Rajput, M. Anas, V. K. Malik, T. Maitra, T. K. Nath and A. Taraphder. *J. Phys.: Condens. Matter* **34** 435801 (2022).
- [29] P. Hohenberg, W. Kohn. *Phys. Rev.* **136**, B864 (1964).
- [30] W. Kohn, L.J. Sham. *Phys. Rev.* **140**, A1133 (1965).
- [31] P.E. Blöchl. *Phys. Rev. B* **50**, 17953 (1994).
- [32] G. Kresse, D. Joubert. *Phys. Rev. B* **59**, 1758 (1999).
- [33] G. Kresse, J. Hafner. *Phys. Rev. B* **47**, 558(R) (1993).
- [34] G. Kresse, J. Furthmüller. *Phys. Rev. B* **54**, 11169 (1996).
- [35] J.P. Perdew, K. Burke, M. Ernzerhof. *Phys. Rev. Lett.* **77**, 3865 (1996).
- [36] H.J. Monkhorst and J.D. Pack *Physical Review B*, **13**, 5188–5192 (1976).
- [37] S.L. Dudarev, G.A. Botton, S.Y. Savrasov; C.J. Humphreys; A.P. Sutton. *Phys. Rev. B* **57**, 1505(1998).

- [38] S. Baroni, S.D. Gironcoli, A.D. Corso, P. Giannozzi. *Rev. Mod. Phys.* **73**, 515 (2001).
- [39] Togo, Atsushi and Isao Tanaka. *Scripta Materialia*, **108**:1–5 (2015).
- [40] Y. Repelin, C. Proust, E. Husson, and J. Beny, *J. Solid State Chem.* **118**, 163 (1995).
- [41] B. Allieri, L. E. Depero, A. Marino, L. Sangaletti, L. Caporaso, A. Speghini, and M. Bettinelli, *Mater. Chem. Phys.* **66**, 164 (2000).
- [42] H. S. Nair, D. Swain, H. N. S. Adiga, C. Narayana, and S. Elizabeth, *J. Appl. Phys.* **110**, 123919 (2011)
- [43] M. Iliev, M. Abrashev, A. Litvinchuk, V. Hadjiev, H. Guo, A. Gupta, *Phys. Rev. B* **75**, 104118 (2007).
- [44] A. P. Ayala, I. Guedes, E. N. Silva, M. S. Augsburger, M. del C. Viola, and J. C. Pedregosa, *J. Appl. Phys.* **101**, 123511 (2007).
- [45] C. L. Bull, D. Gleeson, and K. S. Knight, *J. Phys.: Condens. Matter* **15**, 4927 (2003).
- [46] M. N. Iliev, M. M. Gospodinov, M. P. Singh, J. Meen, K. D. Truong, P. Fournier, and S. Jandl, *J. Appl. Phys.* **106**, 023515 (2009).
- [47] C. Meyer, S. Hühn, M. Jungbauer, S. Merten, B. Damaschke, K. Samwer, and V. Moshnyaga, *J. Raman Spectrosc.* **48**, 46 (2017).
- [48] R.B. Macedo Filho, A. Pedro Ayala, C. William de Araujo Paschoal, *Appl. Phys. Lett.* **102**, 192902 (2013).
- [49] M. Balkanski, R.F. Wallis, E. Haro, *Phys. Rev. B.* **28**, 1928–1934 (1983).
- [50] K.D. Truong, M.P. Singh, S. Jandl, P. Fournier, *J. Phys. Condens. Matter.* **23**, 052202 (2011).
- [51] H.S. Nair, D. Swain, H.N.S. Adiga, C. Narayana, S. Elizabeth, *J. Appl. Phys.* **110**, 123919 (2011),
- [52] R.B. Macedo Filho, A. Pedro Ayala, C. William de Araujo Paschoal, *Appl. Phys. Lett.* **102**, 192902 (2013),

- [53] Kaustuv Manna, R. Sarkar, S. Fuchs, Y. A. Onykiienko, A. K. Bera, G. Aslan Cansever, S. Kamusella, A. Maljuk, C. G. F. Blum, L. T. Corredor, A. U. B. Wolter, S. M. Yusuf, M. Frontzek, L. Keller, M. Iakovleva, E. Vavilova, H.-J. Grafe, V. Kataev, H.-H. Klauss, D. S. Inosov, S. Wurmehl, and B. Büchner, *Phys. Rev. B* **94**, 144437 (2016).
- [54] M. N. Iliev, M. V. Abrashev, A. P. Litvinchuk, V. G. Hadjiev, H. Guo, and A. Gupta, *Phys. Rev. B* **75**, 104118 (2007).
- [55] J.K. Murthy, K.D. Chandrasekhar, S. Murugavel, A. Venimadhav, *J. Mater. Chem. C* **3**, 836e843 (2015),
- [56] X.L. Wang, J. Horvat, H.K. Liu, A.H. Li, S.X. Dou, Spin glass state in Gd₂CoMnO₆ perovskite manganite, *Solid State Commun.* **118**, 27e30 (2001).
- [57] S. Yanez-Vilar, E.D. Mun, V.S. Zapf, B.G. Ueland, J.S. Gardner, J.D. Thompson, et al., *Phys. Rev. B* **84**, 134427 (2011),
- [58] D. Kumar, S. Kumar, and V. G. Sathe, *Solid State Commun.* **59**, 194 (2014).
- [59] Venkata Srinu Bhadrani, B. Rajeswaran, A. Sundaresan and Chandrabhas Narayana . *EPL* **101**, 17008 (2013).
- [60] R. X. Silva, H. Reichlova, X. Marti, D. A. B. Barbosa, M. W. Lufaso, B. S. Araujo, A. P. Ayala and C. W. A. Paschoal. *J. Appl. Phys.* **114**, 194102 (2013).
- [61] S. Venugopalan, M. Dutta, A. K. Ramdas, J. P. Remeika, *Phys. Rev. B* **31**, 1490 (1985).